



## Global and regional evolution of sea surface temperature under climate change



R. Ruela<sup>a</sup>, M.C. Sousa<sup>a</sup>, M. deCastro<sup>b</sup>, J.M. Dias<sup>a,\*</sup>

<sup>a</sup> CESAM, Departamento de Física, Universidade de Aveiro, Portugal

<sup>b</sup> Environmental Physics Laboratory (EphysLab), CIM-UVIGO, Universidade de Vigo, Edificio Campus da Auga, 32004 Ourense, Spain

### ARTICLE INFO

#### Keywords:

SST variability  
CMIP5  
Global warming  
K-means cluster

### ABSTRACT

Sea surface temperature (SST) has important local and remote influence on global climate through the distribution and transport of heat and moisture, which in turn affect precipitation and air temperature patterns across the globe. Thus, this work aims to assess the worldwide regionalization of the SST evolution for the 21<sup>st</sup> century under the influence of climate change by means of: 1) division of the worldwide SST data in regions applying a K-means cluster procedure and validation of the most suitable CMIP5 models by a comparative analysis with SST data from ERA-Interim reanalysis; 2) calculation of SST trends along the 21<sup>st</sup> century and assessment of future SST differences between RCP 4.5 and RCP 8.5 greenhouse gas emission scenarios and historical SST data. Global climate model (GCM) projections show a SST warming worldwide although with different intensity depending on the region. Northern Hemisphere regions present a higher seasonal thermal amplitude comparing with equivalent regions in the Southern Hemisphere. Northern Hemisphere has also a higher annual SST increment than clusters in the Southern Hemisphere, independently of the future time period and climate scenario. The Northern Sub-Tropical cluster (STRN) shows the highest significant increment ( $4.34\text{ }^{\circ}\text{C}$  on RCP 8.5). Under the RCP 4.5 climate scenario, SST trends from 1975 to 2100 range from  $0.075\text{ }^{\circ}\text{C dec}^{-1}$  at South Polar cluster (PRS) to  $0.21\text{ }^{\circ}\text{C dec}^{-1}$  at STRN cluster. Relatively to RCP 8.5 climatic scenario, SST trends change from  $0.13\text{ }^{\circ}\text{C dec}^{-1}$  at PRS cluster to  $0.36\text{ }^{\circ}\text{C dec}^{-1}$  at the North Polar cluster (PRN).

### 1. Introduction

Sea surface temperature (SST) changes are one of the most important sources of uncertainty in future climate changes predictions and analysis (Good et al., 2008). Variations in global and regional SST patterns influence zonal and meridional circulations, which in turn affect the precipitation and air temperature patterns across the globe (Bjerknes, 1969; Hastenrath, 1978; Folland et al., 1986; Rodwell et al., 1999; Chang et al., 2000). Changes in ocean circulation patterns modify the warm and cold water transport patterns around the globe, affecting which species are represented in marine ecosystems, altering migration and breeding patterns, threatening corals, and changing the frequency and intensity of harmful algal blooms (Ostrander et al., 2000). Over the long term, increases in SST could decline the circulation patterns that bring nutrients from the deep sea to surface waters, contributing to declining fish populations, which will affect people who depend on fishing for food or jobs (Pratchett et al., 2004).

Data from the U.K. Meteorological Office Hadley Centre climatology from 1957 to 2006 published in Belkin (2009), establish that most of

the worldwide coasts present an SST increasing, especially in the Subarctic Gyre, in the European Seas and in the East Asian Seas. Studies with daily SST Analysis provided by Optimum Interpolation Sea Surface Temperature (OISST) 1/4 database were also performed. These studies found that more than 71% of the world's coastlines have warmed over the period 1982–2010 (Lima and Wethey, 2012; Rodríguez, 2017). However, this warming magnitude depends on different globe locations, which has led to numerous studies at the regional scale (Gómez-Gesteira et al., 2008; Yoon et al., 2012; Bao and Ren, 2014; Xu et al., 2015; Bouali et al., 2017).

In particular, Gómez-Gesteira et al. (2008) analysed coastal warming by means of satellite-derived SST along the continental Atlantic Arc from 1985 to 2005. These authors detected an inhomogeneous warming trend, ranging from  $3.5\text{ }^{\circ}\text{C century}^{-1}$  at latitudes close to  $48^{\circ}\text{N}$  to  $1.2\text{ }^{\circ}\text{C century}^{-1}$  at latitudes close to  $37^{\circ}\text{N}$ . Yoon et al. (2012) and Bao and Ren (2014) used monthly SST data from the Met Office Hadley Center's (HadISST) for the periods 1950–2007 and 1870–2011, respectively. Yoon et al. (2012) examined western North Pacific SST under the influence of two different types of El Niño (NINO3

\* Corresponding author.

E-mail address: joao.dias@ua.pt (J.M. Dias).

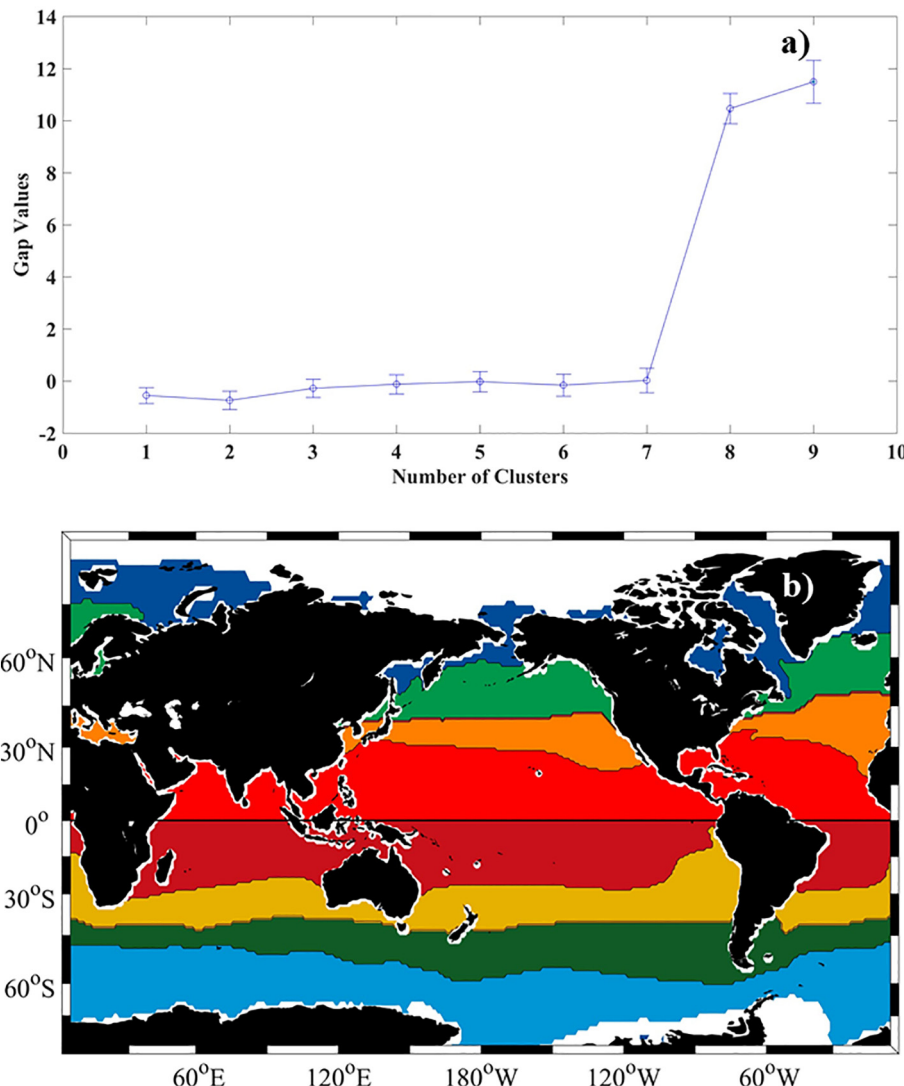


**Fig. 1.** a) Gap values of Era Interim climatology data; b) Worldwide regions based on K-Means cluster analysis with four clusters. Polar (PRN – PRS), Sub-Tropical (STRN – STRS), Tropical (TRN – TRS) and Equatorial (ERN – ERS). White areas correspond to the sea ice.

and NINO4). Their results suggest that the physical processes, responsible for the western North Pacific SST are similar, regardless of different types of El Niño. [Bao and Ren \(2014\)](#) shows that the warming trends of the marginal seas of China during the period 1870–2011 are generally larger than the global and hemispheric averages. Using a Global Circulation Model (GCM), [Caesar et al. \(2018\)](#) identified the weakening of the Atlantic meridional overturning circulation (AMOC) through SST fingerprint from 1870 to 2016. The fingerprint consists of a pattern of cooling in the subpolar Atlantic Ocean and warming in the Gulf Stream region.

As reported by previously studies, SST changes cause different impacts depending on globe location. Thus, several studies were performed in order to assess future SST changes by means of GCMs projections. Firstly, historical SST observations were compared with historical SST data produced by GCMs from the third ([Gillett et al., 2008](#); [Ting et al., 2013](#)) and fifth ([Wang et al., 2014](#); [Chan and Wu, 2015](#)) phase of the Coupled Model Intercomparison Project. These studies concluded that GCMs present a good reproducibility of SST data. Global SST projections also reported general warming, although with different magnitudes ([Xie et al., 2010](#); [He and Soden, 2016](#)).

In this sense, [Shimura et al. \(2015\)](#) used 18 models of CMIP3 with four SST conditions. All the SST patterns show that SST in the future climate increases up to about 3 °C. The North Pacific, especially, shows

a greater increase in temperature than any other region. Moreover, some authors compared CMIP3 and CMIP5 models results. [Pushpadas \(2015\)](#) compared CMIP3 and CMIP5 implementations by multi-model ensembles in Baltic and North Sea. They concluded that the averaged SST in the CMIP3 simulations (~ 2.3 °C in the North Sea and ~ 3.3 °C in the Baltic Sea) is larger than the projected increase for the CMIP5 scenarios (~ 1.7 °C in the North Sea and ~ 2.3 °C in the Baltic Sea).

Based on 19 GCMs CMIP5 under representative concentration pathway 8.5 (RCP 8.5) climatic scenario, [Brown et al. \(2014\)](#) explored the projected SST warming along the equator relative to the edge of the Western Pacific Warm Pool. The authors compared the second halves of the 20<sup>th</sup> (1950–2000) and 21<sup>st</sup> (2050–2100) centuries and found SST anomalies of 2–3 °C for the 3 best models and SST anomalies of 2–5 °C for 11 worst models. In the tropical region, [Huang \(2015\)](#) studied the seasonal SST changes under global warming using 31 models based on the RCP 8.5 and historical runs. The magnitude of the seasonal warming is comparable to the tropical-mean and the annual-mean warming, implying great impacts on global climate changes. [Khalil et al. \(2016\)](#) concluded that forecasts suggest a future warming of 0.004 °C yr<sup>-1</sup> in the Indo Pacific region until 2100 by means of 22 GCMs from the CMIP5 project under the RCP 2.6 scenario.

More recently, [Alexander et al. \(2018\)](#) used 26 models of CMIP5 and 30 simulations from National Center for Atmospheric research Large

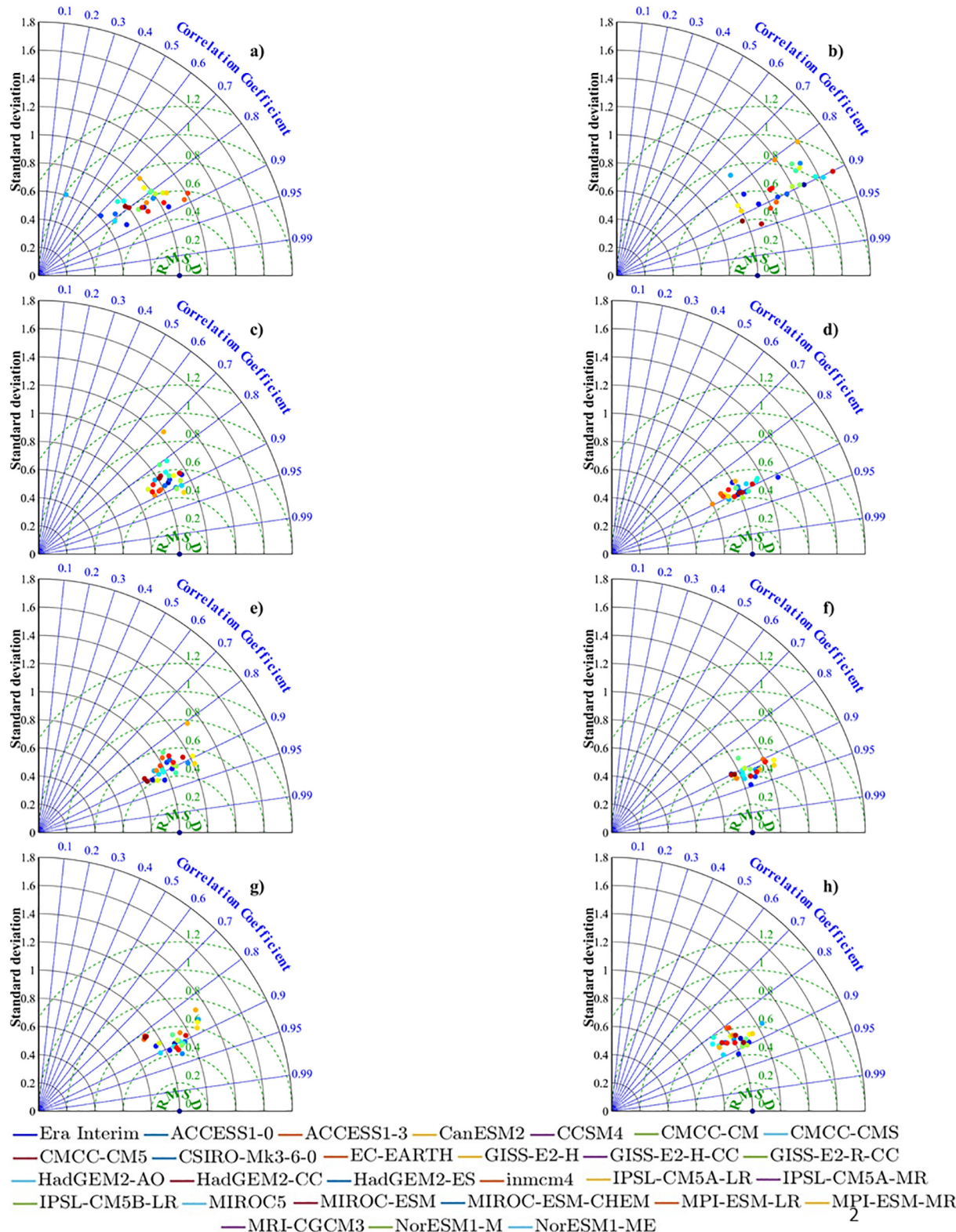


**Fig. 2.** Taylor Diagrams comparing SST data from Era Interim and from different GCMs predictions from the CMIP5 project for each cluster: (a) PRN, (b) PRS, (c) STRN, (d) STRS, (e) TRN, (f) TRS, (g) EQN and (h) EQS. Blue, green and black lines correspond to SD, RMSD and Co respectively.

Ensemble Community Project (CESM – LENS) for the RCP 8.5 climatic scenario to study how climate change affects the mean, variability, and SST extremes in northern oceans areas. The SST trend over the period 1976–2099 is positive over most of the domain, which includes the eastern North Pacific, the North Atlantic and the Arctic Oceans. This

trend varies from approximately  $0.25^{\circ}$  to  $0.5^{\circ}$  decade $^{-1}$  with the strongest warming in the Bering Sea, in the western North Atlantic and in the Norwegian and Barents Seas. The region between Labrador Sea and Southeast of Greenland presents a cooling trend. Considering the SST results of CMES – LENS, SST trend presents a similar pattern and

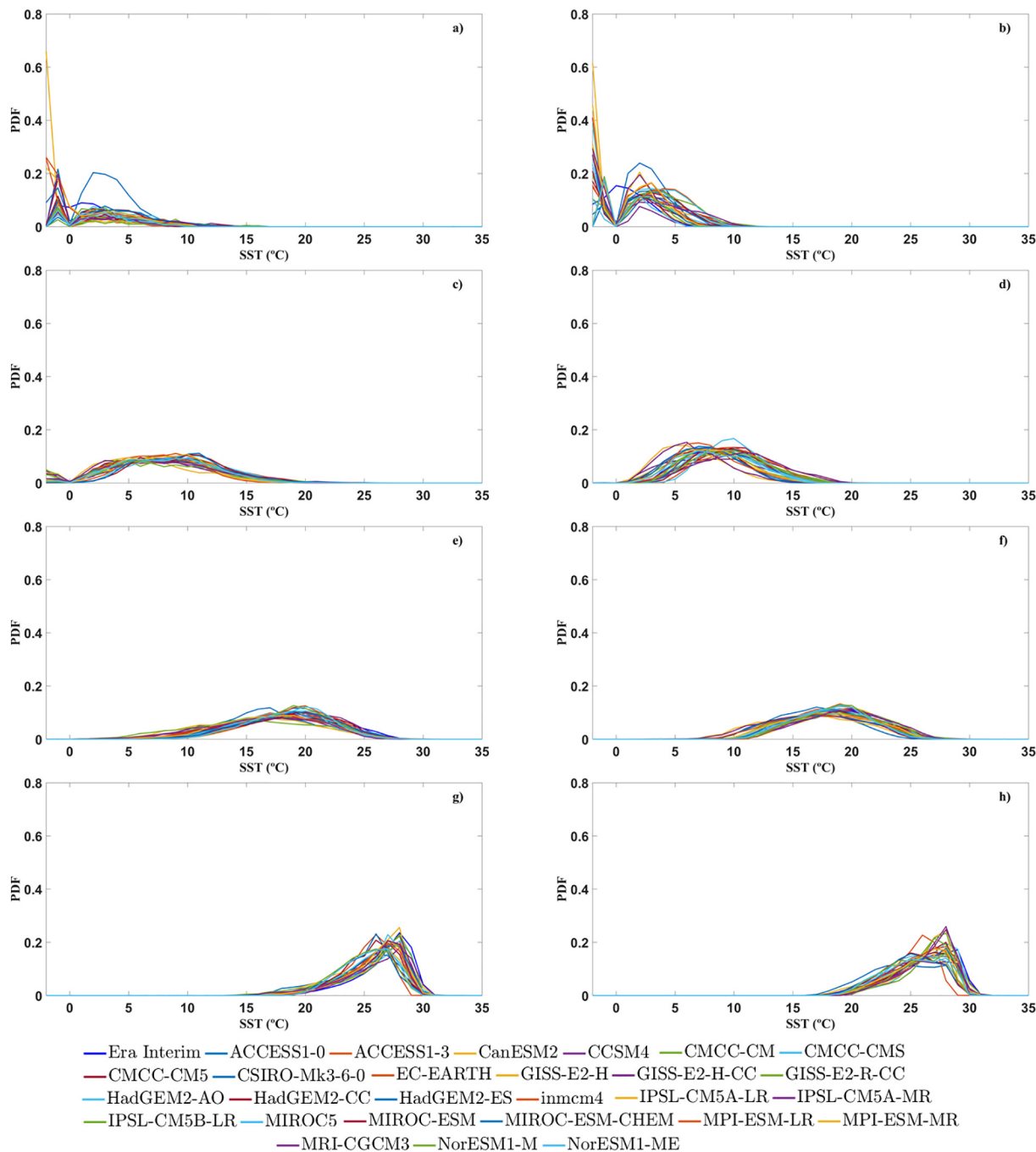


**Fig. 3.** Kernel Density Estimator distribution for each cluster: (a) PRN, (b) PRS, (c) STRN, (d) STRS, (e) TRN, (f) TRS, (g) EQN and (h) EQS.

magnitude, including an absence of warming in the southeast of Greenland, but with stronger warming in the Bering and Greenland Seas.

All these studies provide new insights about the evolution of the SST at different places in the world for the 21<sup>st</sup> century. In order to give a step forward on this subject, the aim of the present study is to perform the worldwide regionalization of the evolution of the SST for the 21<sup>st</sup> century under the climate change context.

## 2. Methodology

### 2.1. SST and sea ice data

Monthly ocean SST data from 1850 to 2100 were obtained from 27

simulations (Table 1 in the supporting information), carried out with GCM developed for the CMIP5 project ([cmip.llnl.gov/cmip5/data\\_portal.html](http://cmip.llnl.gov/cmip5/data_portal.html)).

Historical SST data was extracted from the historical run that covers the period 1850–2005. The historical run was forced by the observed ocean and atmospheric changes, both from anthropogenic and natural sources (Taylor et al., 2012).

Future SST data was taken for two RCP future climate projections: RCP 8.5 and RCP 4.5, which exhibit a radiative forcing of 8.5 and 4.5 W m<sup>-2</sup>, respectively, at the end of the 21<sup>st</sup> century (Moss et al., 2010). For both RCPs the considered period ranged from 2006 to 2100.

Since the CMIP5 GCMs have different horizontal resolutions, SST data were interpolated on a common 1° × 1° grid using the nearest neighbour interpolation method.

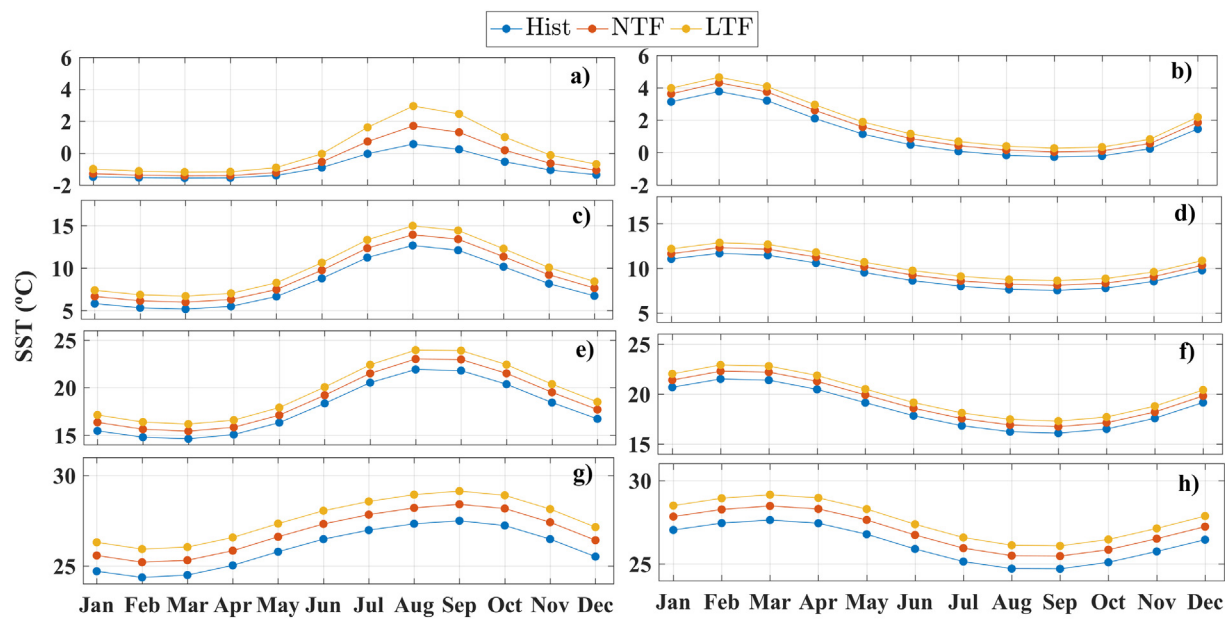


**Fig. 4.** Intra-annual variability of monthly SST means under the RCP 4.5 scenario to PRN (a), PRS (b), STRN (c), STRS (d), TRN (e), TRS (f), ERN (g) and ERS (h) clusters. Blue line represents historical regime (1975–2005), red and yellow lines represent near (2020–2050) and long-term future (2070–2100), respectively.

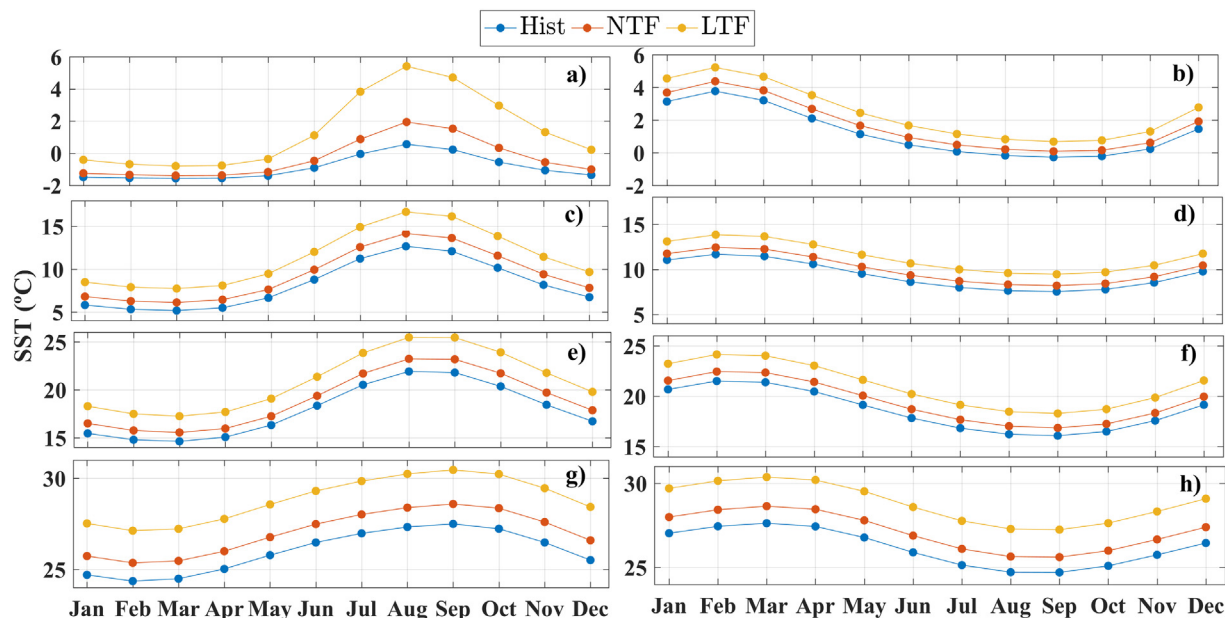


**Fig. 5.** Intra-annual variability of monthly SST means under the RCP 8.5 scenario to PRN (a), PRS (b), STRN (c), STRS (d), TRN (e), TRS (f), ERN (g) and ERS (h) clusters. Blue line represents historical regime (1975–2005), red and yellow lines represent near (2020–2050) and long-term future (2070–2100), respectively.

SST monthly means of daily means data from Era Interim reanalysis (<https://www.ecmwf.int/en/forecasts/datasets/archive-datasets/reanalysis-datasets/era-interim>) between 1975 and 2005 were used as reference SST data. The data assimilation system used to produce Era Interim data is based on the version 3.0 of NEMO ocean model and the NEMOVAR data assimilation system. The NEMO ocean model spatial discretisation is the tripolar ORCA1 configuration of NEMO, which has a horizontal resolution of around  $1^\circ$ , with equatorial refinement. It uses 42 levels in the vertical, 18 of which are in the upper 200 m.

A sea ice mask data was extracted from Era Interim reanalysis for the period 1979–2005, in order to taking into account the polar defrosts. As sea ice area vary widely along the time, it was chosen the year where the sea ice presents higher area. Thus, the sea ice data of 1979 was selected and interpolated. In this work the sea ice area will be

considered constant along the time.

## 2.2. Models selection and data validation

An assessment of the skill of GCMs from CMIP5 to reproduce the worldwide SST was carried out, in order to identify the climate models that best reproduce worldwide SST patterns. In this sense, a comparative analysis between SST data predicted by CGMs and monthly SST data from Era Interim reanalysis was performed. The comparison was done for the period covering 1979–2005.

### 2.2.1. Worldwide SST data division

Ocean areas of the globe were divided in a manageable number of regions, with a simple shape and different climatic regime, by means of

**Table 1**

Differences and respective standard deviation between the annual mean of the climatological SST for the historical (1975–2005) and future periods for RCP 4.5 and RCP 8.5 climatic scenarios.

Regions	RCP 4.5 scenario		RCP 8.5 scenario	
	Near-term future (2020–2050) (°C)	Long-term future (2070–2100) (°C)	Near-term future (2020–2050) (°C)	Long-term future (2070–2100) (°C)
PRN	0.46 ± 0.37	1.03 ± 0.74	0.57 ± 0.44	2.27 ± 1.53
STRN	0.99 ± 0.18	1.84 ± 0.31	1.18 ± 0.23	3.19 ± 0.57
TRN	0.95 ± 0.15	1.79 ± 0.21	1.12 ± 0.18	3.09 ± 0.38
ERN	0.87 ± 0.05	1.60 ± 0.04	1.04 ± 0.06	2.87 ± 0.09
ERS	0.80 ± 0.04	1.44 ± 0.06	0.96 ± 0.04	2.64 ± 0.08
TRS	0.71 ± 0.07	1.30 ± 0.08	0.85 ± 0.08	2.41 ± 0.16
STRS	0.60 ± 0.05	1.12 ± 0.05	0.71 ± 0.05	2.03 ± 0.11
PRS	0.41 ± 0.09	0.70 ± 0.13	0.47 ± 0.10	1.22 ± 0.20

a temporal K-means cluster analysis (Macqueen, 1967; Marta-Almeida et al., 2016; Carvalho et al., 2016). This cluster analysis was performed based on the climatology (1975–2005) created from Era Interim SST data, resulting in a spatial subdivision of the domain in regions with a similar climatic behaviour (magnitude and variability). Additionally, historical SST data from the GCMs were divided following the same subdivision obtained for Era Interim SST data (DeGaetano and Shulman, 1990; Fovell and Fovell, 1993; Molteni et al., 1996; Legg et al., 2002).

The goal of clustering is to capture the natural structure of the data. This methodology was proposed by Marta-Almeida et al. (2016) and Carvalho et al. (2016), being applied on atmospheric properties (air temperature and precipitation). K-means cluster analysis is a non-hierarchical clustering method which starts by computing the centroids for each cluster and then calculates the distances between the current

data vector and each of the centroids, assigning the vector to the cluster whose centroid is closest to it (Marta-Almeida et al., 2016). Since this is a dynamic method, meaning that vectors can change cluster after being assigned to it, this process is repeated until all vectors are assigned to a cluster.

## 2.2.2. Comparison between predictions and observations

For validation purposes and in order to select the best model, the historical SST data from different GCMs and Era Interim data were compared by two statistical methods: Taylor Diagrams and Gaussian Kernel Density Estimator. These analyses were applied for each cluster defined with the cluster analysis.

Taylor Diagram method was applied according to methodology adopted by Sousa et al. (2017). This method is used to indicate the statistical significance of apparent differences and the degree of agreement between GCMs and Era Interim data (Taylor, 2001). Taylor diagrams allow three different measures of uncertainty, Standard Deviation (SD), Correlation (Co) and Root Mean Square Deviation (RMSD). Taylor diagrams parameters were calculated for each cluster and pixel from 1975 to 2005.

The probability density function was calculated using a Gaussian Kernel Density Estimator (Rosenblatt, 1956; Parzen, 1962) with a default bandwidth. Gaussian Kernel Estimator was applied on SST data of each 27 GCMs of CMIP5 and for Era Interim SST data on each cluster and pixel for same SST data of Taylor Diagrams (monthly means between 1975 and 2005). The application of kernel smoothing to the frequency distribution of a data set produces the Kernel density estimate, which is a nonparametric alternative to the fitting of a parametric probability density function. To compare the probability distributions of the observed and predicted variables, the Kolmogorov-Smirnov test was performed (KS-test, Kolmogorov, 1933; Smirnov, 1948).

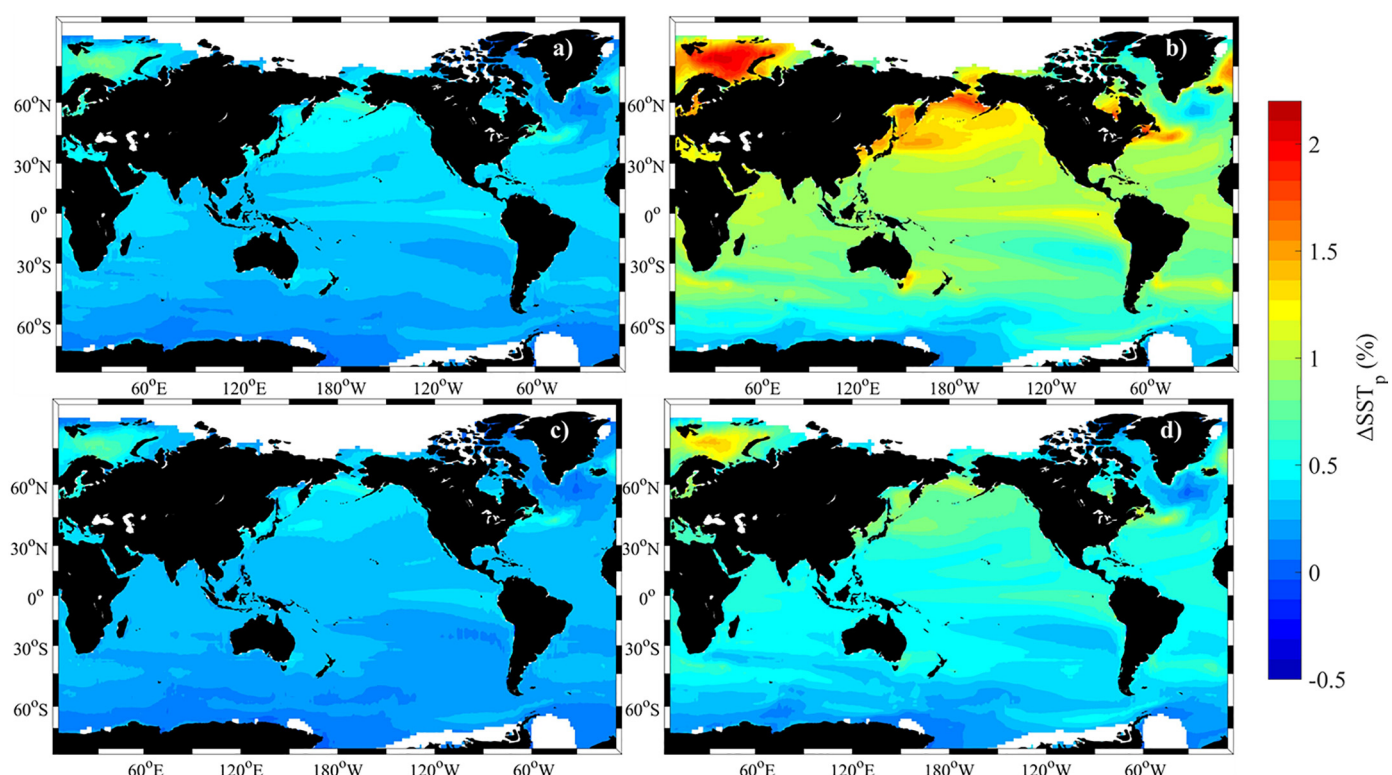


**Fig. 6.** Percentage of SST change between future projections and the historical period (1975–2005): (a) Near-term future projection (2020–2050) under the RCP 8.5 scenario; (b) Long-term future projection (2070–2100) under the RCP 8.5 scenario; (c) Near-term future projection under the RCP 4.5 scenario; (d) Long-term future projection under the RCP 4.5 scenario. White areas correspond to regions with sea ice.

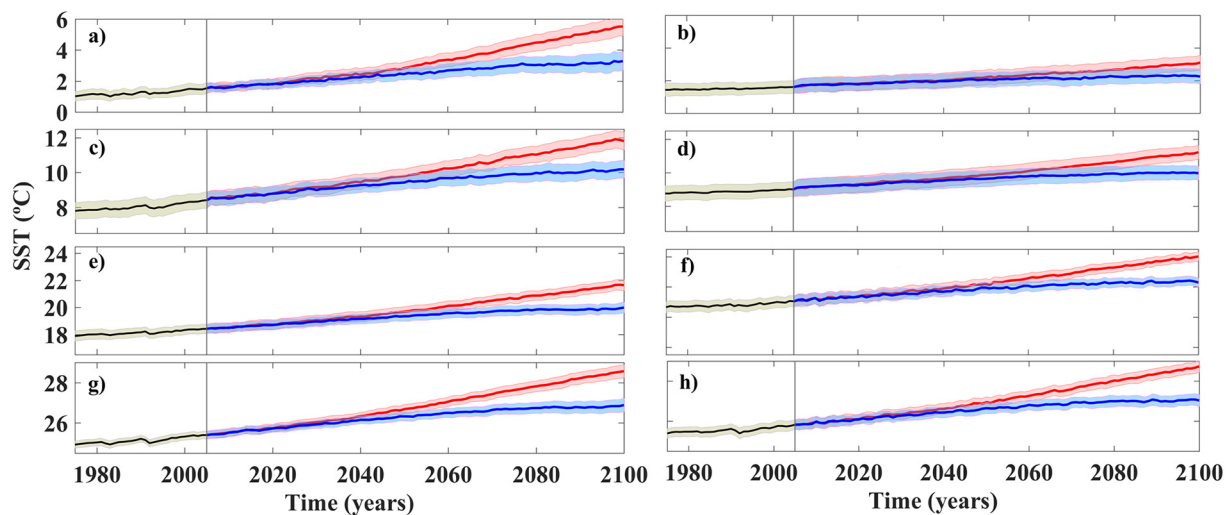


**Fig. 7.** SST trends for each cluster from 1975 to 2100: PRN (a), PRS (b), STRN (c), STRS (d), TRN (e), TRS (f), ERN (g) and ERS (h). Black line represents historical regime, blue (red) line represents RCP 4.5 (RCP 8.5) scenarios. Shaded areas represent deviations.

**Table 2**

SST increments and respective standard deviation for each cluster from 1975 to 2100 for RCP 4.5 and RCP 8.5 climatic scenarios.

Regions	RCP 4.5 scenario (°C)	RCP 8.5 scenario (°C)
PRN	2.40 ± 0.21	4.51 ± 0.24
STRN	2.64 ± 0.25	4.34 ± 0.27
TRN	2.30 ± 0.19	3.95 ± 0.21
ERN	2.18 ± 0.13	3.84 ± 0.13
ERS	1.88 ± 0.11	3.44 ± 0.14
TRS	1.92 ± 0.20	3.49 ± 0.19
STRS	1.41 ± 0.25	2.52 ± 0.24
PRS	0.94 ± 0.22	1.64 ± 0.22

### 2.3. Climate change impacts in future SST variability

SST from the selected GCMs were used to assess future SST changes in the different clusters. Data extracted from the GCMs were organized in a multimodel mean in order to minimize the individual biases (Räisänen and Palmer, 2001; Van Oldenborgh et al., 2013; Rykaczewski et al., 2015; Sousa et al., 2017).

SST differences between the historical period (1975–2005) and each RCP climatic scenario was evaluated by means of the percentage of variation defined as (Eq. 1):

$$\Delta SST(\%)_{(i,j)} = \frac{SST_{f(i,j)} - SST_{p(i,j)}}{SST_{p(i,j)}} \times 100 \quad (1)$$

where  $i$  is the latitude of the point,  $j$  is the longitude,  $SST_f$  is future SST data and  $SST_p$  is historical SST data. This evaluation was carried out both for the near future (2020–2050) and the long-term future (2070–2100).

Following the methodology adopted by Tebaldi et al. (2011), Wang et al. (2015) and Sousa et al. (2017), multimodel SST trends from 1975 to 2100 were calculated for each cluster as the slope of the linear regression. In order to know SST trends for each cluster, the multimodel SST was latitudinal and longitudinally averaged. Additionally, the paired Student's  $t$ -test (Press et al., 1992), which identify the locations of statically significant differences ( $p$ -values lower than 0.05) between future and historical periods, was applied.

## 3. Results and discussion

### 3.1. Worldwide SST data division

The worldwide regions with consistent SST changes (magnitude and variability) were identified through K-means results of Era Interim reanalysis SST data (Fig. 1a).

Gap value measures the difference within intra-cluster variation between the observed and a random uniform distribution data. A large gap statistics means the clustering structure is very far away from the random uniform distribution. The number of clusters ( $k$ ) is the smallest value of  $k$  such that the gap statistic is within one standard deviation of the gap at  $k + 1$  (Tibshirani et al., 2000). Thus, in this study, the optimal  $k$  corresponds to the first local minimum, in this case when gap values of data are nearly constant. This condition was verified when  $k$  is between 1 and 7 (Fig. 1a).

When applying the clustering algorithm to SST data using a  $k$  value of 3 (results not shown), the domain is divided into three regions for each hemisphere. In this case, the Polar and Sub-Tropical regions cannot be separated, although they present significant SST differences. When the number of clusters is increased, more regions can be observed in each hemisphere and therefore the regions obtained will provide a more detailed definition of changes (Carvalho et al., 2016).

Therefore, when using  $k = 4$ , each hemisphere is divided into four regions and the Polar and Sub-Tropical regions can be separated (Fig. 1-b) and changes analysed independently. When using  $k = 5$ , the tropical regions in both hemispheres were sub-divided, and these sub-regions present a small latitudinal extension taking into account the study of regional SST changes under climate change. Relatively to  $k = 6$  and  $k = 7$ , the regions between polar and equatorial regions are sub-divided in regions with less latitudinal extension than sub-divided regions of tropical region when applied  $k = 5$ . Thus,  $k = 4$  fits better the purposes of this study dividing the worldwide SST data into eight clusters: Polar cluster (PRN – PRS), Sub-Tropical cluster (STRN – STRS), Tropical cluster (TRN – TRS) and Equatorial cluster (ERN – ERS) (Fig. 1b).

### 3.2. Comparison between predictions and observations

The GCMs skill to predict future SST for each cluster was analysed comparing numerical predictions for the historical period with Era Interim data. This comparison was performed by means of Taylor Diagrams, the Gaussian Kernel Density Estimator and KS-tests.

The comparison resulting from the Taylor Diagrams shows similar SST patterns both for GCMs and Era Interim data (Fig. 2). In general, all

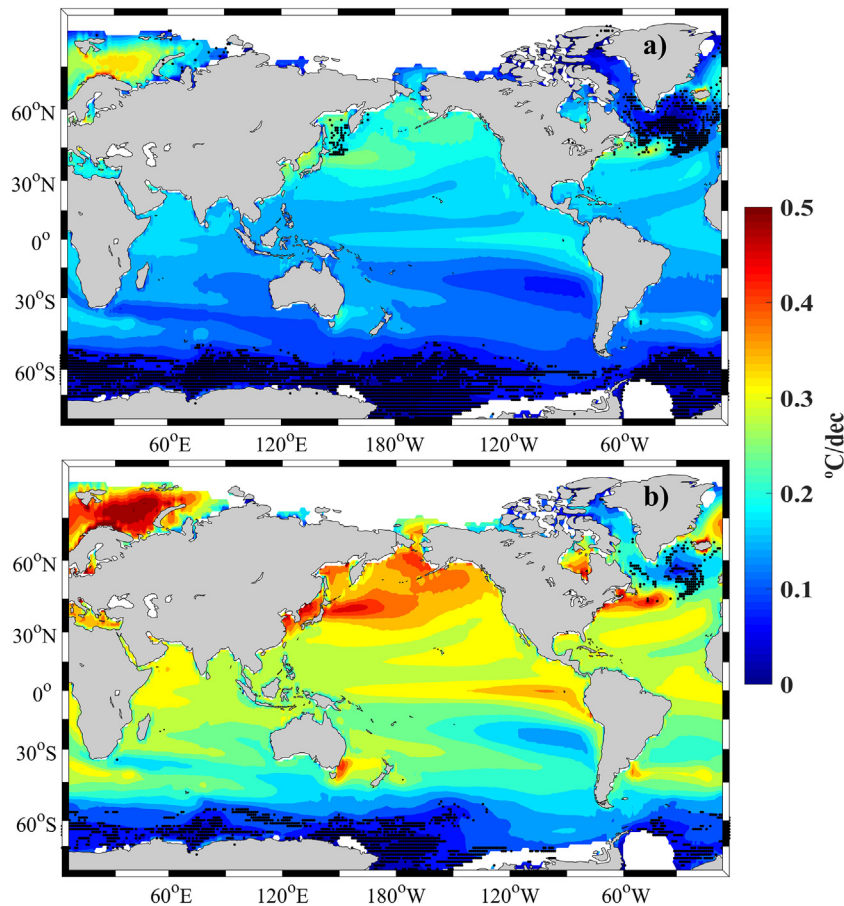


**Fig. 8.** Worldwide SST trend under RCP 4.5 (a) and RCP 8.5 (b) scenarios from 1975 to 2100. Black dots represent coordinates where the significance is less than 95% and white areas correspond to the sea ice.

clusters show a similar dispersion for all GCMs with the exception of PRN (Fig. 2a) and PRS (Fig. 2b) clusters, which show higher scattered between GCMs and Era Interim data. This dispersion is more pronounced in the PRS region (Fig. 2b). TRS cluster is the cluster where most of the GCMs show the Taylor Diagram statistical parameters closest to the optimal values (0 °C for RMSD, 1 °C for SD and 1 for Co).

The Kernel Density Estimator was analysed for all clusters to complement Taylor Diagrams outcomes (Fig. 3). Results show a similar pattern between SST predictions and Era Interim data for all clusters, except for the PRN where SST predicted by three models (CSIRO-Mk3-6-0, MPI-ESM-LR and MPI-ESM-MR) has a different distribution. SSTs simulated by CMIP5 models generally show lower values in the Northern Hemisphere (Fig. 3, left column) than in the Southern Hemisphere (Fig. 3, right column). As expected, SST values increase from Poles to the Equator (reaching values close to 27.5 °C).

A KS-test was used to assess the comparison between predicted and observed SST probability distributions from Kernel Density function (Tables 2 and 3, for North and South Hemisphere respectively, in the supporting information). In the KS-test, high *p*-values or low *d*-values (maximum distance between the cumulative distributions) indicate the null-hypothesis that both groups (numerical predictions and Era Interim data) were sampled from populations with similar distributions. Thus, with this condition verified the prediction data cannot be rejected. According to Marta-Almeida et al. (2016), *p*-values higher than 0.05 (the usual level of significance) indicate that the hypothesis should not be rejected. In the present study, majority of models for different clusters present *p*-values between 0.5 and 1, which are in agreement with the Kernel Density Estimator results (Fig. 3) and justifies the discarding of the CSIRO-Mk3-6-0, MPI-ESM-MR and MPI-ESM-LR models in the analysis of future changes in the SST. Henceforward, in order to

minimize the individual biases, a multimodel mean of SST predictions from 24 models will be considered.

### 3.3. Climate change impacts in future SST variability

The intra-annual variability of the monthly SST was analysed for the historical period (1975–2005) and for near (2020–2050) and long-term future (2070–2100) for all clusters. This analysis was performed considering RCP 4.5 (Fig. 4) and RCP 8.5 (Fig. 5) climatic scenarios. Monthly SST was calculated averaging each month for the whole period (i.e. averaging all Januaries from 1975 to 2005, for the historical period).

The SST seasonality is clearly recognized in both hemispheres with low values during winter months and high during summer months. As expected, future SST values under RCP 8.5 scenario are higher than under RCP 4.5 in all regions and both future periods. In both hemispheres, minimum SST data was found in Polar Regions for the historical regime and maximum in equatorial regions for a long-term future under the RCP 8.5 scenario (Fig. 5). The Northern Hemisphere (Figs. 4 a,c,e,g and Figs. 5 a,c,e,g) present a higher seasonal thermal amplitude than the equivalent regions of the Southern Hemisphere (Figs. 4 b,d,f,h and Figs. 5 b,d,f,h) for all time periods. In the Northern Hemisphere under the RCP 8.5 and for the long-term future, SST ranges from -1.5 °C at the polar region during winter to 32 °C at the equator in September. Under similar conditions in the Southern Hemisphere, SST ranges from 0 °C at the polar region during winter to 32 °C at the equator during August and September.

Differences between the annual mean of the climatological SST for the future and the historical period was calculated for each cluster (Table 1). In general, as expected, the differences between long-term

future and historical regime are larger than differences between near-term future and recent-past. For the long-term future, worldwide SST will have mean increments of 2.46 °C and 1.35 °C under RCP 8.5 and RCP 4.5 scenarios, respectively. Regarding the near-term future, worldwide SST will have mean increments of 0.86 °C and 0.73 °C under RCP 8.5 and RCP 4.5 scenarios, respectively. In particular, clusters in the Northern Hemisphere has a higher annual SST increment (2.27 °C – 3.19 °C) than clusters in the Southern Hemisphere (1.22 °C – 2.64 °C) independently of the future time period and climate scenario.

Results obtained in this work are in agreement with previous IPCC predictions, which show that ocean surface warming will vary considerably between the emission scenarios, ranging from 1 °C to more than 3 °C for subtropical and tropical regions (IPCC, 2013). Particularly on Northern Hemisphere clusters and ERS cluster, the maximum of SST increments present similar magnitudes as reported on other studies (Brown et al., 2014; Matear et al., 2014). However, when comparing SST increment with Shimura et al. (2015) results, the value found in this study for equatorial clusters (ERN and ERS) presents a smaller magnitude. Nevertheless, SST increments found by Shimura et al. (2015) present a higher standard deviation (0.21 °C – 0.38 °C) comparing with those obtained in this study. This SST increment difference between both studies can be explained by Pushpadas (2015), which compared SST results from CMIP3 and CMIP5 projects and concluded that CMIP3 presents higher SST increments than CMIP5, however, GCM of CMIP5 shows minor standard deviation.

The percentage of SST change worldwide between near and long-term future and the historical period was represented in Fig. 6 under both RCP scenarios.

In general, the largest warming is found in high latitudes of the Northern Hemisphere for near and long-term futures and RCP scenarios. The percentage of SST change for the near-term future shows a similar pattern under both RCP scenarios although slightly higher under the RCP 8.5 mainly in the equatorial region (Figs. 6a and 6c). Considering RCP 8.5 scenario, SST shows percentages of change between 0.1% and 1.0% worldwide for the near future (Fig. 6a). The percentage of SST change for the long-term future show, in general, higher values worldwide under the RCP 8.5 scenario (Fig. 6b).

The percentage of SST change associated with the long-term future under the RCP 8.5 scenario (Fig. 6b), decreases from values close to 2% at the PRN cluster to 0.5% for the region between Australia and South America and for Indo-Pacific regions. In contrast, this percentage of SST change decreases between 1.25% and 0.25% under the RCP 4.5 (Fig. 6d). These regional variations in the projected amplitude of SST change can be influenced by ocean circulation as well as by surface heating (Timmermann et al., 2007; DiNezio et al., 2009; Yin et al., 2009; Xie et al., 2010; Yin et al., 2010). Considering the lower grid resolutions of GCMs on polar regions (PRN and PRS), the percentage of SST changes in these regions present higher deviations. On PRS cluster, percentages of SST change close to zero or even negatives could be explained by this grid limitation.

The percentage of SST change presents a significant spatial variation in Tropical and Sub-Tropical clusters. These variations can be explained by the inter-decadal variability of upper ocean temperatures, which is larger in mid-latitudes, particularly in the Northern Hemisphere than in the tropics (Wang et al., 2010).

The inter-annual evolution of the SST for each cluster from 1975 to 2100 under both RCP scenarios is represented in Fig. 7. A significant increasing in SST will occur in all clusters and RCP scenarios.

Clusters in the Northern Hemisphere (Figs. 7a, c, e, g) will present higher SST increments than those in the Southern Hemisphere (Figs. 7b, d, f, h). These increments are show in Table 2.

Considering both RCP scenarios, the SST increments decrease from PRN to PRS cluster. Minimum and maximum of SST increment in the Northern Hemisphere occur on ERN (3.84 °C) and PRN (4.51 °C) for the RCP 8.5 scenario. In the Southern Hemisphere, SST increases will range from 1.64 °C (minimum in PRS) to 3.49 °C (maximum in TRS) for the

RCP 8.5 scenario. Nevertheless, according to Taylor Diagram results the PRN (maximum of SST increment) and PRS (minimum of SST increment) are the clusters with worse proximity patterns between GCMs and Era Interim Data. One other hand, the TRS (maximum of SST increment in the South Hemisphere) present the best proximity to the optimal values of Taylor Diagrams (0 °C for RMSD, 1 °C for SD and 1 for Co).

Comparing both future scenarios (RCP 4.5 and 8.5), the differences between SST trends are higher for the clusters of the Northern Hemisphere than their equivalents in the Southern Hemisphere, corroborating a higher SST warming in Northern Hemisphere. In fact, SST trends differences between RCPs decrease from the North Pole to the South Pole. Considering both RCP's scenarios, Northern Hemisphere clusters present divergent patterns from 2075 until 2100, except ERN cluster that do not present overlap in SST trend from 2060 to 2100. Southern Hemisphere presents divergent patterns from 2070 for ERS and TRS, and from 2090 for the STRS cluster.

Worldwide SST trends from 1975 and 2100 were computed under RCP 4.5 and RCP 8.5 scenarios (Fig. 8 a, b, respectively). Trends are statistically robust across climate models and are significant in almost all regions, with exception of the South Pole and the North Atlantic regions (black points in Fig. 8).

Overall, a significant worldwide SST warming is projected under both RCP scenarios, although being less intense in the South Pole. A general warming along coastal areas will be also observed, in line with previous studies based on historical SST data, which reported an increasing SST trend during the second half of the last century (Lima and Wethey, 2012; Barton et al., 2013). Both scenarios present higher SST trends in the Northern Hemisphere, namely in the Subtropical Region, in agreement with time series shown in Fig. 7. Maximum SST warming rates of 0.5 °C dec<sup>-1</sup> would be observed in the Northern Hemisphere under the RCP 8.5 scenario. This value is in line with SST trends calculated by Alexander et al. (2018), varying from approximately 0.25° to 0.5 °C decade<sup>-1</sup> in northern ocean areas. The strongest warming (1976–2099) was found in the Bering Sea, (western North Atlantic) and in the Norwegian and Barents Seas, with same SST trends found in the present work. Relatively to RCP 4.5 scenario, the maximum SST trend (0.35 °C dec<sup>-1</sup>) occurs close to Norway. However, regions with strongest warming in RCP8.5 scenario are also present in RCP4.5, but with lower SST trends.

In general, SST trends present an intensification under the RCP 8.5 scenario compared to the RCP 4.5 scenario, mainly between 30°N and 30°S, presenting an average trend of approximately 0.3 °C dec<sup>-1</sup> in this area. SST trends present a small increment comparing with results obtained by Rodríguez (2017), that analysed several coastal areas around the world. The authors estimated a significant general ocean warming rate higher than 0.2 °C dec<sup>-1</sup> in La Guajira, lower than 0.2 °C dec<sup>-1</sup> in Java and between 0.1 °C dec<sup>-1</sup> and 0.2 °C dec<sup>-1</sup> in Yucatan.

Finally, SST trends in the South Pole vary from 0.1 to 0.2 °C dec<sup>-1</sup> under both RCP scenarios in agreement with results obtained in Fig. 7.

#### 4. Conclusions

Different GCMs from the CMIP5 project were used to analyse SST variability worldwide for the 21st century. An assessment of the skill of these GCMs on predicting SST was performed by a comparative analysis with Era Interim SST data. According to the statistical analysis of Taylor Diagrams and Kernel Distribution Estimator, it was possible to conclude that most of GCMs reproduce real SST variations for the historical period. However, some GCMs (CSIRO-Mk3-6-0, MPI-ESM-MR and MPI-ESM-LR) presented poor model performance and were discarded. Thus, a multimodel mean of the selected models was considered to minimizes individual model bias and errors.

The SST seasonal cycle is clearly observed in the future in both hemispheres regardless the RCP scenario considered. Under the RCP 8.5 scenario, SST ranges from –1.5 °C in the PRN during winter to 32 °C in

the ERN in August, while in the Southern Hemisphere, SST ranges from 0 °C during winter months in the PRS to 32 °C in the ERN during summer. Clusters in the Northern Hemisphere present a higher seasonal thermal amplitude comparing with equivalent clusters of the Southern Hemisphere.

The assessment of SST changes under global warming effects was carried out, showing a future worldwide warming. Differences between the annual mean of the climatological SST for future periods and the historical period (1975–2005) will be more evident in STRN (3.19 °C) and TRN (3.09 °C) regions under the RCP 8.5 for the long-term future (2070–2100). Also, high SST trends will be found in the PRN cluster, where warming will have higher impacts, but with higher deviations probability on account of lower grid resolution on this cluster.

SST increments will be higher in the Northern Hemisphere regardless the RCP scenario, mainly in the STRN, presenting superior impact. The higher increments for RCP 4.5 and RCP 8.5 climatic scenarios are respectively 2.40 °C and 4.51 °C in the PRN, 2.64 °C and 4.34 °C in the STRN, 2.30 °C and 3.95 °C in the TRN and 2.18 °C and 3.84 °C in the ERN clusters. All these increments are in line with worldwide trends (Fig. 8).

The future SST warming projected worldwide may have implications in zonal and meridional circulations, which in turn will affect the precipitation and air temperature patterns across the globe. The SST warming is an indicator of global warming, and consequently of the increasing of greenhouses emissions concentrations, like carbon dioxide. Thus, levels of dissolved carbon will continue to increase and will change the chemistry of seawater, turning it more acid. As referred early, with oceans acidity increase, certain organisms, such as coral and shellfish, will have difficulties to build their skeletons and shells. These effects could substantially affect the biodiversity and productivity of ocean ecosystems. However, SST increase variability depends on the different globe locations. Thus, this study may be used as a starting point to downscaling studies, that may string new insights on regional scales.

## Acknowledgements

The second author is funded by national funds (OE), through FCT, I.P., in the scope of the framework contract foreseen in the numbers 4, 5 and 6 of the article 23, of the Decree-Law 57/2016, of August 29, changed by Law 57/2017, of July 19. Thanks are due to FCT/MCTES for the financial support to (UIDP/50017/2020+ UIDB/50017/2020), through national funds. This study was partially funded under the project AquiMap (MAR-02.01.01-FEAMP-0022) cofinanced by MAR2020 Program, Portugal 2020 and European Union though the European Maritime and Fisheries Fund.

## Declaration of Competing Interest

The authors declare that they have no known competing financial interests or personal relationships that could have appeared to influence the work reported in this paper.

## Appendix A. Supplementary data

Supplementary data to this article can be found online at <https://doi.org/10.1016/j.gloplacha.2020.103190>.

## References

- Alexander, Michael A., Scott, James D., Friedland, Kevin D., Mills, Katherine E., Nye, Janet A., Pershing, Andrew J., Thomas, Andrew C., 2018. Projected sea surface temperatures over the 21st century: changes in the mean, variability and extremes for large marine ecosystem regions of northern oceans. *Elem Sci Anth* 6 (1), 9.
- Bao, B., Ren, G., 2014. Climatological characteristics and long-term change of SST over the Marginal Seas of China. *Cont. Shelf Res.* 77, 96–106.
- Barton, E.D., Field, D.B., Roy, C., 2013. Canary current upwelling: more or less? *Prog. Oceanogr.* 116, 167–178.
- Belkin, I.M., 2009. Rapid warming of large marine ecosystems. *Prog. Oceanogr.* 81 (1–4), 207–213.
- Bjerknes, J., 1969. Atmospheric teleconnections from the equatorial pacific 1. *Mon. Weather Rev.* 97 (3), 163–172.
- Bouali, M., Sato, O.T., Polito, P.S., 2017. Temporal trends in sea surface temperature gradients in the south atlantic ocean. *Remote Sens. Environ.* 194, 100–114.
- Brown, J.N., Langlais, C., Sen, A.S., 2014. Projected sea surface temperature changes in the equatorial pacific relative to the warm pool edge deep-sea research II projected sea surface temperature changes in the equatorial pacific relative to the warm pool edge. *Deep-Sea Res. II* 113, 1–12.
- Caesar, L., Rahmstorf, S., Robinson, A., Feulner, G., 2018. Observed fingerprint of a weakening Atlantic Ocean overturning circulation. *Nature* 556, 191–196.
- Carvalho, M.J., Melo-Gonçalves, P., Teixeira, J.C., Rocha, A., 2016. Regionalization of Europe based on a K-means cluster analysis of the climate change of temperatures and precipitation. *Phys. Chem. Earth* 94, 22–28.
- Chan, D., Wu, Q., 2015. Attributing observed SST trends and subcontinental land warming to anthropogenic forcing during 1979–2005. *J. Clim.* 28 (8), 3152–3170.
- Chang, P., Saravanan, R., Ji, L., Hegerl, G.C., 2000. The effect of local sea surface temperatures on atmospheric circulation over the tropical atlantic sector. *J. Clim.* 13 (13), 2195–2216.
- DeGaetano, A.T., Shulman, M.D., 1990. A climatic classification of plant hardiness in the United States and Canada. *Agric. For. Meteorol.* 51 (3–4), 333–351.
- DiNezio, P.N., Clement, A.C., Vecchi, G.A., Soden, B.J., Kirtman, B.P., Lee, S.K., 2009. Climate response of the equatorial pacific to global warming. *J. Clim.* 22 (18), 4873–4892.
- Folland, C.K., Palmer, T.N., Parker, D.E., 1986. Sahel rainfall and worldwide sea temperatures, 1901–85. *Nature* 320, 602.
- Fovell, R.G., Fovell, M.Y.C., 1993. Climate zones of the conterminous United states defined using cluster analysis. *J. Clim.* 6 (11), 2103–2135.
- Gillet, N.P., Stott, P.A., Santer, B.D., 2008. Attribution of cyclogenesis region sea surface temperature change to anthropogenic influence. *Geophys. Res. Lett.* 35 (9), 1–5.
- Gómez-Gesteira, M., deCastro, M., Alvarez, I., Gesteira, J.L. Gómez, 2008. Coastal sea surface temperature warming trend along the continental part of the Atlantic Arc (1985–2005). *J. Geophys. Res.* 113, C04010. <https://doi.org/10.1029/2007JC004315>
- Good, P., Lowe, J.A., Rowell, D.P., 2008. Understanding uncertainty in future projections for the tropical atlantic: relationships with the unforced climate. *Clim. Dyn.* 32 (2–3), 205–218.
- Hastenrath, S., 1978. On modes of tropical circulation and climate anomalies. *J. Atmos. Sci.* 35, 2222–2231.
- He, J., Soden, B.J., 2016. The impact of SST biases on projections of anthropogenic climate change: a greater role for atmosphere-only models? *Geophys. Res. Lett.* 43 (14), 7745–7750.
- Huang, P., 2015. Seasonal changes in tropical SST and the surface energy budget under global warming projected by CMIP5 models. *J. Clim.* 28 (16), 6503–6515.
- IPCC, 2013. Climate change 2013: the physical science basis. The Fifth Assessment Report 5, 1552.
- Khalil, I., Atkinson, P.M., Challenor, P., 2016. Looking back and looking forwards: historical and future trends in seasurface temperature (SST) in the indo-pacific region from 1982 to 2100. *Int. J. Appl. Earth Obs. Geoinf.* 45, 14–26.
- Kolmogorov, A.N., 1933. ‘Sulla determinazione empirica di una legge di distribuzione’. *G. Dell Ist. Ital. Degli Attuari* 4, 83–91.
- Legg, T.P., Mylne, K.R., Woolcock, C., 2002. Use of medium-range ensembles at the Met Office 1: PREVIN - A system for the production of probabilistic forecast information from the ECMWF EPS. *Meteorol. Appl.* 9 (3), 255–271.
- Lima, F.P., Wethay, D.S., 2012. Three decades of high-resolution coastal sea surface temperatures reveal more than warming. *Nat. Commun.* 3, 1–13.
- Macqueen, J., 1967. Some methods for classification and analysis of multivariate observations. In: Proceedings of the Fifth Berkeley Symposium on Mathematical Statistics and Probability. 1 (233), pp. 281–297.
- Marta-Almeida, M., Teixeira, J.C., Carvalho, M.J., Melo-Gonçalves, P., Rocha, A.M., 2016. High resolution WRF climatic simulations for the iberian peninsula: model validation. *Phys. Chem. Earth* 94, 94–105.
- Matear, R.J., Chamberlain, M.A., Sun, C., Feng, M., 2014. Climate change projection for the western tropical pacific ocean using a high-resolution ocean model: implications for tuna fisheries. *Deep-Sea Res. II* 113, 22–46.
- Molteni, F., Buizza, R., Palmer, T.N., Petroliagis, T., 1996. Analysis of the ECMWF ensemble prediction system: methodology and validation. *Q. J. R. Meteorol. Soc.* 122, 73–119.
- Moss, R.H., Edmonds, J.A., Hibbard, K.A., Manning, M.R., Rose, S.K., Van Vuuren, D.P., Carter, T.R., et al., 2010. The next generation of scenarios for climate change research and assessment. *Nature* 463 (7282), 747–756.
- Ostrander, G.K., Armstrong, K.M., Knobbe, E.T., Gerace, D., Scully, E.P., 2000. Rapid transition in the structure of a coral reef community: the effects of coral bleaching and physical disturbance. *Proc. Natl. Acad. Sci. U. S. A.* 97 (10), 5297–5302.
- Parzen, E., 1962. On estimation of a probability density function and mode. *Ann. Math. Stat.* 33 (3), 1065–1076.
- Pratchett, M.S., Wilson, S.K., Berumen, M.L., McCormick, M.I., 2004. Sublethal effects of coral bleaching on an obligate coral feeding butterflyfish. *Coral Reefs* 23 (3), 352–356.
- Press, W.H., Teukolsky, S.A., Vetterling, W.T., Flannery, B.P., 1992. Numerical Recipes. Cambridge University Press, Cambridge, U.K.
- Pushpadas, D., 2015. Projected climate change impacts on North Sea and Baltic Sea: CMIP3 and CMIP5 model based scenarios. *Biogeosci. Discuss.* 12, 12229–12279.
- Räisänen, J., Palmer, T.N., 2001. A probability and decision-model analysis of a

- multimodel ensemble of climate change simulations. *J. Clim.* 14 (15), 3212–3226.
- Rodríguez, R.V., 2017. Worldwide evolution of upwelling and its influence on SST trends. Phd. Universidad de Vigo 162.
- Rodwell, M.J., Rowell, D.P., Folland, C.K., 1999. Oceanic forcing of the wintertime North Atlantic oscillation and european climate. *Nature* 398 (6725), 320–323.
- Rosenblatt, M., 1956. Remarks on some nonparametric estimates of a density function. *Ann. Math. Stat.* 27 (3), 832–837.
- Rykaczewski, R.R., Dunne, J.P., Sydeman, W.J., García-Reyes, M., Black, B.A., Bograd, S.J., 2015. Poleward displacement of coastal upwelling-favorable winds in the ocean's eastern boundary currents through the 21st century. *Geophys. Res. Lett.* 42 (15), 6424–6431.
- Shimura, T., Mori, N., Mase, H., 2015. Future projection of ocean wave climate : analysis of sst impacts on wave climate changes in the Western North Pacific. *Am. Meteorol. Soc.* 2012, 3171–3190.
- Smirnov, N., 1948. Table for estimating the goodness of fit of empirical distributions. *Ann. Math. Stat.* 19 (2), 279–281.
- Sousa, M.C., DeCastro, M., Alvarez, I., Gomez-Gesteira, M., Dias, J.M., 2017. Why coastal upwelling is expected to increase along the Western Iberian Peninsula over the next Century? *Sci. Total Environ.* 592, 243–251.
- Taylor, K.E., 2001. Summarizing multiple aspects of model performance in a single diagram. *J. Geophys. Res.-Atmos.* 106 (D7), 7183–7192.
- Taylor, K.E., Stouffer, R.J., Meehl, G.A., 2012. An overview of CMIP5 and the experiment design. *Bull. Am. Meteorol. Soc.* 93 (4), 485–498.
- Tebaldi, C., Arblaster, J.M., Knutti, R., 2011. Mapping model agreement on future climate projections. *Geophys. Res. Lett.* 38 (23), 1–5.
- Tibshirani, R., Walther, G., Hastie, T., 2000. Estimating the number Os clusters in a data set via the gap statistic. *J. R. Statist. Soc. B, Part2* 63, 411–423.
- Timmermann, A., Okumura, Y., An, S.I., Clement, A., Dong, B., Guilyardi, E., Hu, A., et al., 2007. The influence of a weakening of the atlantic meridional overturning circulation on ENSO. *J. Clim.* 20 (19), 4899–4919.
- Ting, M., Kushnir, Y., Li, C., 2013. North atlantic multidecadal SST oscillation: external forcing versus internal variability. *J. Mar. Syst.* 133, 27–38.
- van Oldenborgh, G.J., Doblas Reyes, F.J., Drijfhout, S.S., Hawkins, E., 2013. Reliability of regional climate model trends. *Environ. Res. Lett.* 8 (1).
- Wang, C., Zhang, L., Lee, S.K., Wu, L., Mechoso, C.R., 2014. A global perspective on CMIP5 climate model biases. *Nat. Clim. Chang.* 4 (3), 201–205.
- Wang, D., Gouhier, T.C., Menge, B.A., Ganguly, A.R., 2015. Intensification and spatial homogenization of coastal upwelling under climate change. *Nature* 518 (7539), 390–394.
- Wang, M., Overland, J.E., Bond, N.A., 2010. Climate projections for selected large marine ecosystems. *J. Mar. Syst.* 79 (3–4), 258–266.
- Xie, S.P., Deser, C., Vecchi, G.A., Ma, J., Teng, H., Wittenberg, A.T., 2010. Global warming pattern formation: sea surface temperature and rainfall. *J. Clim.* 23 (4), 966–986.
- Xu, H., Kim, H.M., Nye, J.A., Hameed, S., 2015. Impacts of the North Atlantic oscillation on sea surface temperature on the Northeast US continental shelf. *Cont. Shelf Res.* 105, 60–66.
- Yin, J., Schlesinger, M.E., Stouffer, R.J., 2009. Model projections of rapid Sea-Level rise on the Northeast Coast of the United States. *Nat. Geosci.* 2, 262.
- Yin, J., Griffies, S.M., Stouffer, R.J., 2010. Spatial variability of sea level rise in twenty-first century projections. *J. Clim.* 23 (17), 4585–4607.
- Yoon, J., Yeh, S.W., Kim, Y.H., Kug, J.S., Min, H.S., 2012. Understanding the responses of sea surface temperature to the two different types of El Niño in the Western North Pacific. *Prog. Oceanogr.* 105, 81–89.